Article

Spectroscopic Study on CdS/Ni/KNbO$_3$: Confirming Ni Effect to Photocatalytic Activity

Su Young Ryu,* Tai Kyu Lee, and Michael R. Hoffmann*

Cite This: *ACS Omega* 2023, 8, 35173−35182

Read Online

ACCESS | Metrics & More | Article Recommendations | SI Supporting Information

ABSTRACT: Herein, we report the structural and photophysical properties of CdS/Ni/KNbO$_3$ composites with a quantum yield for photocatalytic H$_2$ generation that is CdS and Ni amount dependent. The nonstoichiometric KNbO$_3$ (1:1.1) structure indicates the defect at the K site, which is Ni-occupied during its deposit process. It exhibits a tendency like a Ni-doped characteristic up to 0.1 wt % Ni and then forms a Ni cluster in case the Ni amount exceeds 0.1 wt %. The related structural and photophysical properties of CdS/Ni/KNbO$_3$ are examined with Fourier transform infrared, X-ray diffraction, ultraviolet−visible absorption, and luminescence spectral analysis. It demonstrates the CdS/Ni/KNbO$_3$ composites to be an efficient light conversion caused by efficient charge/electron transfer between KNbO$_3$ and CdS via doped Ni. The photocatalytic activity of CdS/Ni/KNbO$_3$ exhibits a CdS and Ni amount dependency. The best photocatalytic activity for H$_2$ generation is obtained with 0.1 wt % Ni and 2.9 wt % CdS as it gradually declines with the excess Ni amount than 0.1 wt % caused by a formed Ni cluster.
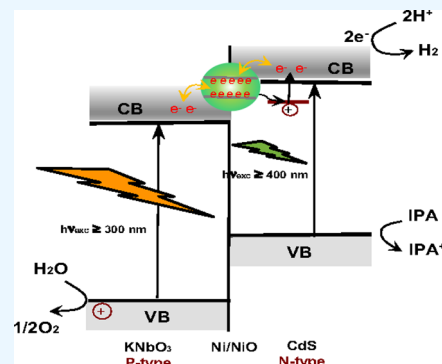
1. INTRODUCTION

Hydrogen production from water using a semiconductor photocatalyst has attracted considerable interest in the conversion of solar energy. Honda and Fujishima discovered that water can be photo-electrochemically decomposed into hydrogen (H$_2$) and oxygen (O$_2$) using a TiO$_2$ electrode under UV light irradiation in 1972.[1] Since then, many of the metal oxide semiconductors such as Nb$_2$O$_5$, Ta$_2$O$_5$, ZrO$_2$, SrTiO$_3$, SrNb$_2$O$_7$, and SrTa$_2$O$_7$, etc. have been discovered to be activity for water splitting into H$_2$ and O$_2$. Especially, K$_4$Nb$_6$O$_{17}$ has attracted considerable interest in the redox reaction due to an unique layered structure consisting of two characteristic interlayers (I and II) showing different physical and chemical properties.[2−4] Indeed, Ni/K$_4$Nb$_6$O$_{17}$ and Pt/K$_4$Nb$_6$O$_{17}$ that are intercalated Ni or Pt in the interlayer I as a co-catalyst have been reported to have a great photocatalytic activity for water splitting into H$_2$ and O$_2$ caused by delocalized charge carriers in the NbO$_6$ octahedral structure.[2−5] However, most metal oxide semiconductors have photocatalytic activity under UV light only ($\lambda \leq 400$ nm, ~5% of solar light) due to their wide band gap since the valence band mainly consists of O 2p orbitals, whose electrical potential is about 3 eV vs NHE.[6] Thus, a lot of efforts have been made to develop photocatalysts responding to visible light corresponding ~42% of solar light.

CdS, an n-type semiconductor with E_{BG} = 2.4 eV, has been known as a photocatalyst responding to visible light for H$_2$ generation.[7,8] The photocatalytic activity of CdS can be improved by combining to other semiconductors having a different energy level and band gap, for example, TiO$_2$/CdS,[9] ZnO/CdS, ZnS/CdS,[10,11] and K$_4$Nb$_6$O$_{17}$/CdS compo-

sites,[7,12,13] resulted in efficient charge separation as a Z-schematic photocatalysis system. The separated charge carriers can prevent or retard the charge recombination, resulting in improved photocatalytic activity.[8,14,15]

In this study, we reveal the photoinduced electron transfer mechanism on the CdS/Ni/KNbO$_3$ composite by a diffuse reflectance infrared Fourier transform (DRIFT), UV−vis absorption, and luminescence spectroscopic study. The electronic band structure of KNbO$_3$ has been studied in various aspects of research.[6,16,17] According to KNbO$_3$ structural study, the valence band (VB) of KNbO$_3$ is derived primarily from oxygen 2p with the contribution of Nb 4d to the low and middle parts, while the conduction band (CB) is mostly derived from Nb 4d orbitals. The calculations of CB generally agree to predict two separated energy structures of Nb 4d t_{2g} and e$_g$ due to a lift of degeneracy for the Nb 4d orbitals in the octahedral NbO$_6$ site. On the other hand, the electron states of potassium, K, are mostly located in the upper part of the conduction band (CB) and the lower part of the valence band (VB). Therefore, the electronic property of KNbO$_3$ is mainly dependent on the Nb and O, even though the potassium, K, still indirectly affects the electron environ-
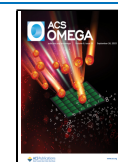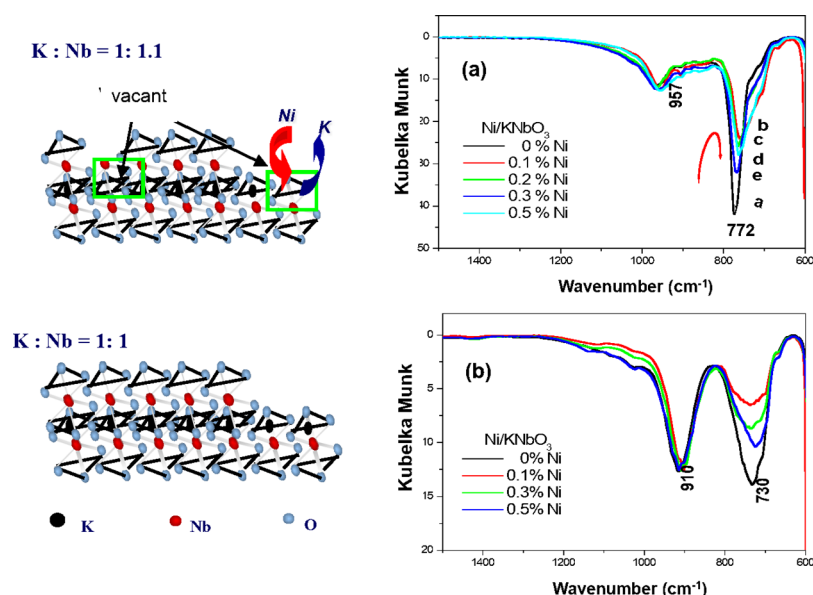
Figure 1. IR spectra of the nonstoichiometric (a) and the stoichiometric (b) structure of $KNbO_3$ corresponding to Ni deposit amounts. The significant spectral change is obtained with the bridged O−Nb−O vibrational mode at 772 and 730 cm^{-1} for each of nonstoichiometric and stoichiometric $KNbO_3$ structures.

ment of Nb and O. The electron density of the valence band (VB) increases when Nb 4d states strongly hybridize with the O 2p orbital, and this hybridization seems to enhance a ferroelectric distortion. Indeed, the ferroelectric distortion induced by displacement or vacancy of a cation site in the structure leads to change of the net dipole moment or polarization in unit volume.[6,16,17]

For this study, we synthesized $KNbO_3$ in a nonstoichiometric mixture of K_2CO_3 and Nb_2O_5 (1:1.1), which creates a vacancy at K^+ site and affects the structural and photophysical properties of $CdS/Ni/KNbO_3$ composite.[14,15] The hybrid composites combined an n-type CdS and a p-type $KNbO_3$ would be an ideal design not only potential advantage by a band gap engineering but also efficient charge/electron transfer at the p-n junction, occurring charge diffusion in the interface. The Ni located in the interface between $KNbO_3$ and CdS takes a crucial role as a route of charge and electron transfer, resulting in a Z-scheme characteristic mechanism for the photocatalytic reaction.[14,15]

2. EXPERIMENTAL SECTION

2.1. Preparation of Materials. $KNbO_3$ is prepared by conventional solid-state reactions at high temperatures as follows: K_2CO_3 (Aldrich) and Nb_2O_5 (99.9%, Aldrich) (1:1.1 nonstoichiometric) are mixed and ground in a mortar and then pressed with 4000 psi. The pressed pellet is calcined at 1025 °C in air for 10 h with a heating temperature ramp of 200 °C/ h. The $Ni/KNbO_3$ is prepared by Ni^{2+} deposit on the $KNbO_3$ surface, which suspends $KNbO_3$ powder in $Ni(NO_3)_2$ aqueous solution for 1 day. The $Ni^{2+}/KNbO_3$ is heat-treated at 500 °C for 2 h under a H_2 atmosphere, followed by additional O_2 treatment at 200 °C for 1 h in a closed gas circulation system. $Ni/KNbO_3$ indicates an immediate color change from green to gray with H_2 treatment at 500 °C. The composite materials of $CdS/KNbO_3$ and $CdS/Ni/KNbO_3$ are prepared as follows: 1 g of $KNbO_3$ or $Ni/KNbO_3$ is stirred in 20 mL of 10 mM cadmium acetate ethanol solution for 24 h; then, sulfurization is carried out by the addition of 20 mL of 10 mM Na_2S ethanol

solution and kept stirring for 7 days at room temperature. The powder was washed with ethanol and distilled water several times and subsequently dried at 130 °C.

2.2. Analytical Methods and Instruments. The X-ray diffraction (XRD) pattern is measured with a Philips diffractometer (X'pert Pro) with Cu-Kα radiation. UV−vis diffuse reflectance spectra are recorded on a Shimadzu UV-2101PC with an integrating sphere attachment (Shimadzu ISR-260) using Ba_2SO_4 powder as an internal reference. The UV−vis absorption spectrum is evaluated by the Kubelka−Munk function of the diffuse reflectance:

$$\frac{K}{S} = \frac{(1-r)^2}{2r} \tag{1}$$

where K and S are absorption and scattering coefficients, respectively, and r is the diffuse reflectance. The steady-state emission spectrum is measured with a scanning SLM-AMINCO 4800 spectrofluorometer, which enables the corrected spectra by using a Rhodamine B as a quantum counter. The fs-mode locked Ti−sapphire laser is used as a light source for the study of CdS emission, which generates a 388 nm laser pulse with frequency doubling of the fundamental 776 nm laser pulse having 80 MHz repetition rate by a second harmonic generation (SHG) technique. The emitting photons from CdS are collected by a streak camera. The spectrum of diffuse reflectance infrared Fourier transform (DRIFT) is acquired using a Bio-Rad FTS-45 spectrometer with a liquid N_2-cooled MCT detector as collected at the 8 cm^{-1} resolution using a diffuse reflectance accessory of Spectra-Tech Collector. The sample is held in the sample cup of a Spectra-Tech high temperature environment chamber (HTEC) that could be resistively heated to 1000 K and the gas in the chamber evacuates to 10 μTorr. The structure and chemical composition of materials are analyzed with a field emission scanning electron microscope (LEO 1550 VP FESEM) that is equipped with an energy dispersive spectrometer (EDS). The XPS is obtained with an M-probe surface spectrometer (VG Instruments) using monochromatic Al Kα X-rays (1486.6 eV).

The photocatalysis is performed by using a collimated output of a high-pressure 500 W Hg-Xe arc lamp as a light source in combination with a 400 nm cutoff filter. The evolved H_2 is analyzed using gas chromatography (HPG1800A) with a thermal conductivity detector (TCD).

3. RESULTS AND DISCUSSION

3.1. Structural Properties of Stoichiometric and Nonstoichiometric KNbO₃.

The $KNbO_3$ structures synthesized at the 1:1 and 1:1.1 mole ratios of K_2CO_3 to Nb_2O_5 are identified by analysis of the XRD pattern, as shown in Figure S1. The stoichiometric $KNbO_3$ (1:1) indicates the orthorhombic $KNbO_3$ structure. The deposit process of Ni and CdS to $KNbO_3$ (1:1) does not affect the $KNbO_3$ skeletal structure as it indicates an identical XRD pattern. On the other hand, the nonstoichiometric structure of $KNbO_3$ (1:1.1) generates a flawed $KNbO_3$ structure, as shown in the characteristic layered structural peaks of $K_4Nb_6O_{17}\cdot3H_2O$ at 10, 28, 41, and 47, whose peak intensity is affected by the amount of Ni deposited on the surface of $KNbO_3$ (1:1.1).

Figure 1 exhibits the comparative IR spectra of two $KNbO_3$ structures corresponding to Ni deposit amounts. The nonstoichiometric $KNbO_3$ (a) indicates to have a higher vibrational energy than that of the stoichiometric $KNbO_3$ (b) as follows: the stretching modes of a nonbridged Nb–O and a bridged O–Nb–O are detected at 959 and 772 cm^{-1}, respectively, for the nonstoichiometric $KNbO_3$ structure (a), while the stoichiometric $KNbO_3$ (b) indicates those at 910 and 730 cm^{-1} with similar intensity. An apparent spectral change is observed at the bridged O–Nb–O caused by a Ni^{2+} deposit, resulting in a decreased peak intensity. The Ni effect appears in different aspects depending on the structure. For example, the nonstoichiometric $KNbO_3$ structure (a) exhibits the peak shift from 772 to 756 cm^{-1} with the broadening effect, indicating a decreased vibrational energy as $\Delta E = 16$ cm^{-1}. On the other hand, the Ni effect to the stoichiometric $KNbO_3$ (b) exhibits a decreased peak intensity at 730 cm^{-1} without significant energy change. Since the nonstoichiometric $KNbO_3$ supposedly creates the vacancy at the K^+ site, Ni^{2+} may occupy the vacancy during the process of Ni deposit, resulting in asymmetric bond strength with the bridged O–Nb–O caused by a charge sharing of one oxygen with adjacent Ni^{2+} as we assumed. The most significant change is obtained with 0.1 wt % Ni and then restored peak intensity gradually in case the Ni amount exceeds 0.1 wt %. We assumed that it is due to a formed Ni cluster.

Hereafter, the nonstoichiometric $KNbO_3$ (1:1.1) will be denoted as $KNbO_3$ because no conflict exists anymore since the present study is carried out using $KNbO_3$ (1:1.1) only.

3.2. Photophysical Properties with the Electronic Structure of CdS/Ni/KNbO₃ Composites.

The UV–vis diffuse reflectance spectra of $KNbO_3$, Ni(0.1 wt %)/$KNbO_3$, CdS/$KNbO_3$, CdS/Ni(0.1 wt %)/$KNbO_3$, and Q-size CdS colloids are exhibited in Figure 2. Based on the UV–vis absorption spectrum, the band gap of $KNbO_3$ is obtained as 3.25 eV (±0.005) as calculated in Tauc's method using a conversion factor between band gap energy (eV) and wavelength (nm). The 0.1 wt % Ni deposited on $KNbO_3$ exhibits a weak absorption in the overall wavelength range between 380 and 750 nm. The CdS that deposited on the surface of $KNbO_3$ is identified as nanosize particles (or clusters) by the TEM image as shown in Figure S2. The absorption band edge of CdS/$KNbO_3$ and CdS/Ni(0.1 wt
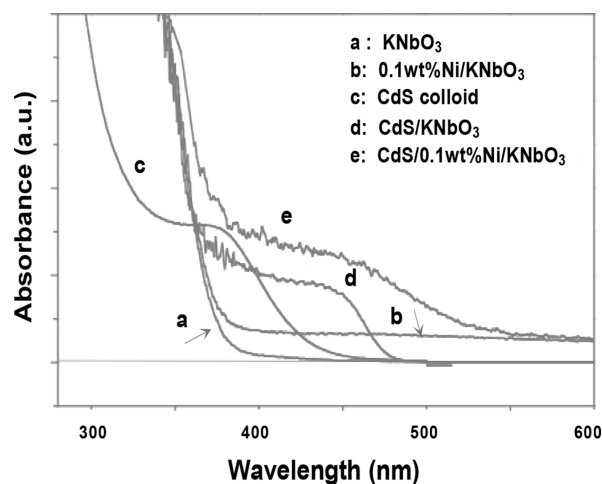

Figure 2. UV–vis diffuse reflectance spectra of $KNbO_3$, Ni(0.1 wt %)/$KNbO_3$, CdS/$KNbO_3$, CdS/Ni(0.1 wt %)/$KNbO_3$, and CdS colloids in ethanol.

%)/$KNbO_3$ is obtained at 478 and 540 nm, respectively. The red-shifted band edge with CdS/Ni(0.1 wt %)/$KNbO_3$ is probably caused by a surface plasmon effect with the doped Ni, which causes coherent electron oscillation at the interface between CdS and $KNbO_3$.

The spectral analysis of the UV vis absorption in Figure 3 is performed corresponding to the Ni deposit process as follows: (a)-a is the absorption spectrum of $Ni(NO_3)_2\cdot6H_2O$ as a Ni precursor; (a)-b, the absorption spectrum of Ni^{2+} that is physically adsorbed on the surface of $KNbO_3$ as measured with the dried sample after immersion of $KNbO_3$ in $Ni(NO_3)_2$ aqueous solution for 1 day; (a)-c, the absorption spectrum of Ni/$KNbO_3$ after H_2 treatment at 500 °C. In detail, the absorption peaks of $Ni(NO_3)_2\cdot6H_2O$ at 390 and 655 nm in Figure 3(a)-a are attributed to the transition of $^3A_{2g}$ (^3F) → $^3T_{1g}$ (^3P) and $^3A_{2g}$ (^3F) → $^3T_{1g}$ (^3F), which are relevant to the transitions of divalent Ni ions, respectively.[18] The deposit of Ni^{2+} on $KNbO_3$ without H_2 treatment indicates a spectral change that is band-shifted from 390 to 450 nm and 655 to 740 nm, respectively, as shown in Figure 3(a)-b (cut at 700 nm). The absorption bands at 450 and 740 nm are assigned to the transitions of $^3A_{2g}$ (^3F) → $^1T_{2g}$ (^1D) for the former and $^3A_{2g}$ (^3F) → $^1E_{1g}$ for the latter, indicating a change of spin multiplicity from triplet to singlet that is basically addressed to the forbidden transition by a particular selection rule. However, the process of forbidden transition is allowed at a lower rate at a higher level of approximation (e.g., magnetic dipole, electric quadrupole).[19] The change of Ni energy states is more likely a diffusion of Ni^{2+} into $KNbO_3$, resulting in more stabilized Ni energy states caused by a charge transfer between Ni^{2+} and $KNbO_3$ structure rather than the formation of NiO.[20,21] The absorption spectrum of Ni^{2+} fades by a treated hydrogen at 500 °C. Instead, weak and broad absorption appears in the wavelength range between 380 and 700 nm, as shown in Figure 3(a)-c. This phenomenon is surely due to the reduction of Ni^{2+} to Ni^0, and the weak and broad absorption is probably caused by a localized surface plasmon effect. Figure 3(b) evidently exhibits the increased surface plasmon absorption corresponding to an increased Ni amount.[22]

$KNbO_3$ and Ni/$KNbO_3$ are examined to be hardly active for photocatalytic H_2 generation even under UV + visible light irradiation ($\lambda \geq 320$ nm). According to Neumann et al., the
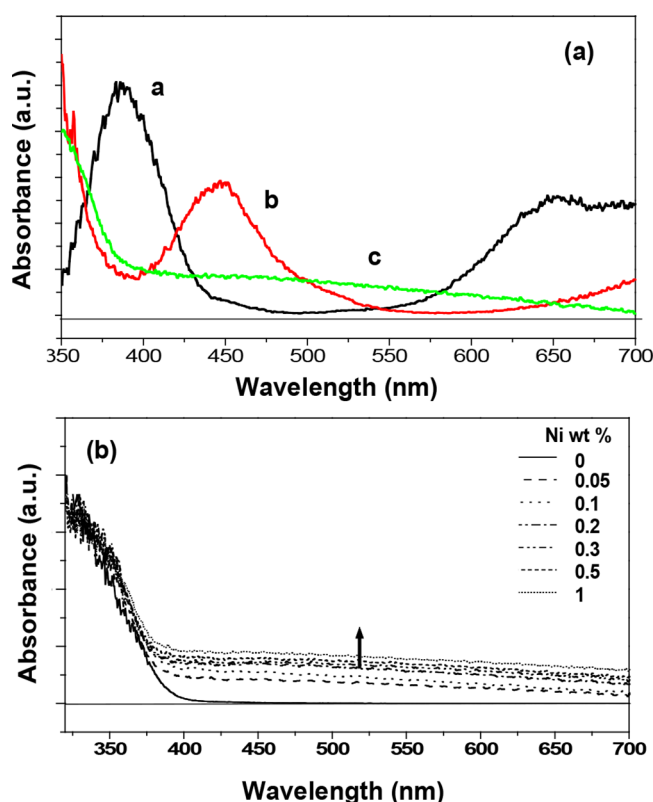
Figure 3. (a) UV−vis diffuse reflectance spectra of Ni species corresponding to the Ni deposit process: **a** (black), the absorption spectrum of $Ni(NO_3)_2 \cdot 6H_2O$ powder as a precursor of Ni; **b** (red), the Ni^{2+} deposited on the surface of $KNbO_3$ before H_2 treatment; **c** (green), $Ni/KNbO_3$ after H_2 treatment at 500 °C for 2 h, followed by O_2 treatment at 200 °C for 1 h. (b) UV−vis diffuse reflectance spectra of $Ni/KNbO_3$ corresponding to the Ni amount of 0, 0.05, 0.1, 0.2, 0.3, 0.5, and 1.0 wt %, respectively.

cubic $KNbO_3$ has a d^5 electron configuration for Nb and consists of the valence band having a strong d-band character due to the evidential hybridization with O $2p$ and the conduction band with unoccupied Nb $4d$ states in the study of the density of states (DOS).[17] On the other hand, Duan et al. revealed that the bottom of the conduction band is mostly derived from Nb $4d$ (LUMO) while the top of the valence band dominantly consists of O $2p$ (HOMO), indicating that the band gap energy varied from 3.1 to 3.8 eV (vs NHE) depending on the phase of $KNbO_3$.[6,16,17,23] The potential of valence and conduction bands for the orthorhombic $KNbO_3$ is determined in between $-0.26 \sim 0$ eV for CB and $3 \sim 3.26$ eV for VB (vs NHE at pH = 0) from the band gap energy of ca. ~ 3.26 eV, which is insufficient potential to reduce H^+ to H_2 (refer to Figure 6).[14,23−25]

On the other hand, the hybrid composites, $CdS/KNbO_3$ and $CdS/Ni/KNbO_3$, exhibit fine photocatalytic activity for H_2 production with a benefit of band gap engineering with CdS consisting of the band edges that enable abundant visible light absorption. Indeed, the potential of conduction and valence bands of CdS is higher than that of $KNbO_3$ due to the higher energy states of Cd $4d$ and S $3p$ than those of Nb $4d$ and O $2p$, respectively. Consequently, the $CdS/KNbO_3$ composite consisting of a different band gap and potential energy has a big advantage for the photocatalysis with efficient charge separation between CdS and $KNbO_3$ as constructed in a Z-schematic photocatalysis system. As a result, the significant

enhancement of H_2 production is obtained with $CdS/Ni/KNbO_3$ due to the crucial role of Ni for efficient charge/electron transfer at the interface between CdS and $KNbO_3$, which resulted in a retardation/prevention of electron−hole recombination.[24]

The mechanism of the internal photo-induced charge/electron transfer is examined with a spectral analysis of the $KNbO_3$ emission corresponding to Ni and CdS deposit amounts. Figure 4(a) shows the emission spectra of $KNbO_3$
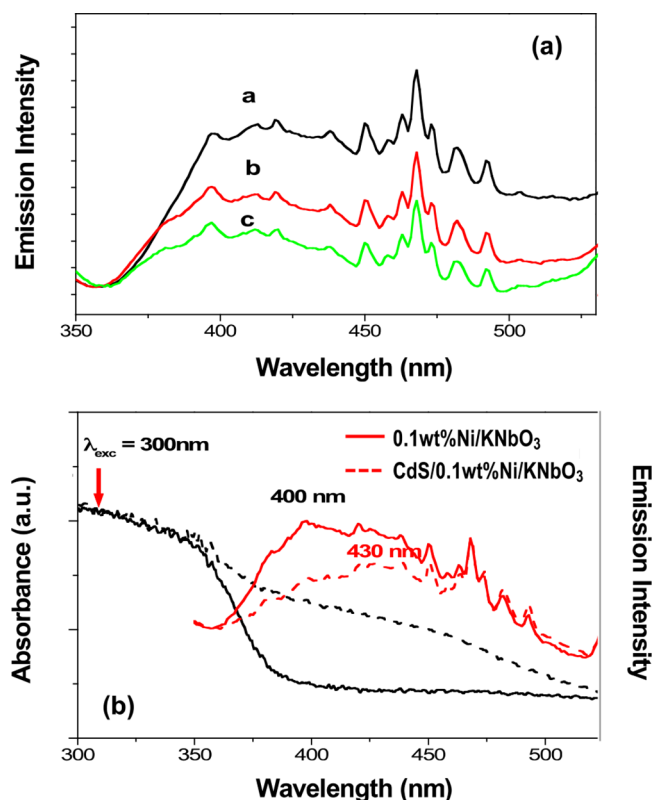
Figure 4. (a) Emission spectra of $KNbO_3$ corresponding to the Ni deposit amount: a, 0%; b, 0.1 wt %; c, 0.3 wt %. (b) Comparative absorption (black) and emission spectra (red) of Ni(0.1 wt %)/$KNbO_3$ (solid) and $CdS/Ni(0.1$ wt %)/$KNbO_3$ (dot). All emission spectrum is obtained with 300 nm light excitation at the room temperature.

corresponding to the Ni deposit amounts of 0, 0.1, and 0.3 wt %, respectively. $KNbO_3$ indicates a broad emission around 400 nm with strong vibronic structural bands in the wavelength range between 450 and 500 nm, whose energy spacing is between 300 and 430 cm^{-1}.[26] The spectral change is detected with a Ni deposit resulted in a decreased emission intensity depending on Ni amounts, indicating an electron/charge transfer reasonably from $KNbO_3$ to Ni. Figure 4(b) exhibits the $KNbO_3$ emission spectra obtained with Ni(0.1 wt %)/$KNbO_3$ comparing with and without CdS deposits. It indicates a spectral change with the CdS deposit, which quenches the emission around 400 nm where the CdS absorption occurred, as shown likely by a peak shifting from 400 to 430 nm. It is more likely caused by a charge/electron transfer to the deposited CdS. On the other hand, the conduction band of CdS is estimated as -0.55 eV vs NHE, and it is about $-0.29 \sim -0.55$ eV higher potential than that of $KNbO_3$. Although CdS may not be suitable energetically to

accept electrons directly from CB of $KNbO_3$, it would be possible to apply an indirect charge/electron transfer via Ni as an intermediator. Hence, we conclude that the quenched $KNbO_3$ emission is caused by a charge/electron transfer to CdS via Ni.[27] In detail, the photoexcited electrons by a 300 nm light irradiation on the $Ni/KNbO_3$ are rapidly relaxed to the emissive states of $KNbO_3$, and some of them might transfer to a doped Ni as shown by quenched emission corresponding to Ni amounts. In case of the $CdS/Ni(0.1 wt \%)/KNbO_3$ composite, the quenched $KNbO_3$ emission at the energy region around 400 nm is detected, where CdS absorption occurred. We attributed it to a charge/electron transfer from $KNbO_3$ to CdS via Ni.

The CdS emission is examined with $CdS/Ni/KNbO_3$ composites corresponding to Ni amounts of 0.1 and 0.3 wt % (Figure 5). It is carried out using a 388 nm laser pulse as a

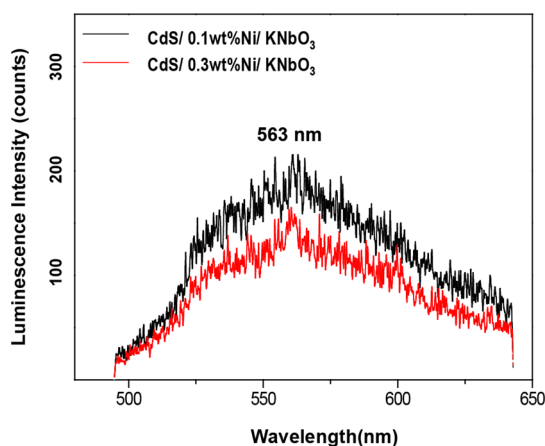**Figure 5.** Emission spectra of CdS obtained with $CdS/Ni/KNbO_3$ composites corresponding to Ni deposit amounts of 0.1 and 0.3 wt %, respectively, by 388 nm laser pulse photoexcitation.

light source and collected the emitted photons by using a streak camera because of the difficulty in detecting the CdS emission by using a conventional spectrofluorometer equipped with a lamp as a light source. The photoexcited electrons of CdS by a 388 nm laser pulse undergo fast nonradiative relaxation to the CdS trap states, followed by a radiative relaxation from the trap states to the ground state, as detected by the emission around 563 nm.[24,27,28] The CdS emission tends to decrease the intensity with an increased Ni amount, as shown in comparison of 0.1 and 0.3 wt % Ni deposited $CdS/Ni/KNbO_3$ composites. Indeed, the intensity of the emission is correlated with the number of radiative electrons and their retention time at the emissive states. For instance, Kamat and Shanghavi reported the CdS emission that is quenched by inter-particle electron transfer to the Au cluster in the composite of the CdS/Au cluster, and the quenching effects greatly increase with the increased amount of the core Au cluster.[29] As we detected an identical quenching effect for the CdS emission with the 0.3 wt % Ni deposited $CdS/Ni/KNbO_3$ composite, it is most likely due to the inter-particle electron transfer from the CdS to Ni cluster that is identified in excess Ni amount than 0.1 wt % (refer to Figure 1).

The luminescence study for $KNbO_3$ and CdS with $CdS/Ni/KNbO_3$ composites leads us to convince the $CdS/Ni/KNbO_3$ composite as an efficient light conversion system with a crucial role of Ni in the interface between CdS and $KNbO_3$, exhibiting

a photo-induced electron relay with efficient charge/electron transfer between $KNbO_3$ and CdS via Ni.

The suggested Z-schematic diagram for the photo-induced electron transfer mechanism with a photocatalytic H_2 production is exhibited in Figure 6. In detail, the UV light
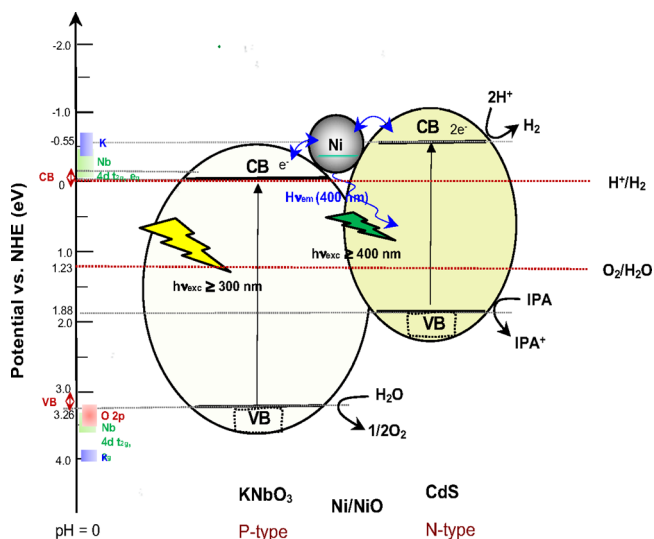
Figure 6. Suggested schematic diagram for the photo-induced electron relay in the $CdS/Ni/KNbO_3$ composite as a Z-Scheme photocatalysis mechanism.

irradiation ($\lambda_{exc} < 380$ nm) to $CdS/Ni/KNbO_3$ composite induced the photo-generated electrons on the conduction band of $KNbO_3$, followed by a nonradiative charge/electron transfer to CdS via Ni as seen in the quenched $KNbO_3$ emission around 400 nm, promoting H_2 generation at the CdS. Under visible light irradiation ($\lambda_{exc} \geq 400$ nm), the H_2 generates at the conduction band (CB) of CdS, while capturing the holes by IPA in the valence band (VB) of CdS. Under UV + visible light irradiation ($\lambda \geq 320$ nm), it proceeds as a Z-schematic photocatalysis mechanism as a combination of two processes of $KNbO_3$ and CdS.

3.3. Photocatalytic H_2 Production with $CdS/Ni/KNbO_3$ Composites. We investigate the photocatalytic H_2 production with $CdS/Ni/KNbO_3$ composites that is CdS and Ni amount dependent.[24] Since the UV−vis diffuse reflectance spectra of $CdS/Ni/KNbO_3$ composites indicate an enhanced absorbance in the visible region with an increased CdS amount, it is predicted that 4.7 wt % CdS composite is the best photocatalytic activity among the 2.3, 2.9, and 4.7 wt % CdS based on visible light utilization (Figure 7(a) inset). However, the photocatalytic H_2 generation is in the order of 2.9 > 2.3 > 4.7 wt % CdS composite, as shown in Figure 7(a). Based on this, the photocatalytic hydrogen production is carried out further with 2.9 wt % CdS deposit to the $Ni/KNbO_3$ that is 0, 0.1, 0.3, 0.5, 1.0 wt % Ni-deposited, respectively, and the result is exhibited in Figure 7(b). The best catalytic activity indicates 0.1 wt % Ni and 2.9 wt % CdS in the $CdS/Ni/KNbO_3$ with a hydrogen production rate of 203.5 μmol/g h under visible light irradiation ($\lambda_{exc} \geq 400$ nm).[24] The photocatalytic activity of $CdS/Ni/KNbO_3$ maintains the initial hydrogen generation rate as the first order kinetics for a whole photolysis period of 3 days.

On the other hand, the UV−vis diffuse reflectance spectra of $CdS/KNbO_3$ and $CdS/Ni/KNbO_3$ composite comparing
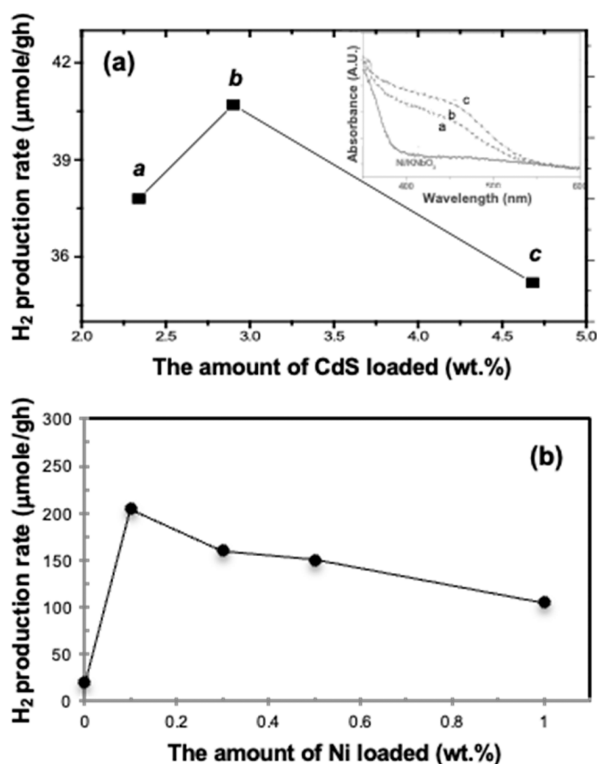
Figure 7. (a) Photocatalytic hydrogen production rates obtained with CdS/Ni/KNbO₃ composites corresponding to the CdS amount. Inset is UV−vis diffuse reflectance spectra of CdS/Ni/KNbO₃ corresponding to the CdS amount: a, 2.3 wt %; b, 2.9 wt %; c, 4.7 wt %. (b) Photocatalytic hydrogen production rates obtained after 2.9 wt % CdS deposit on Ni/KNbO₃ that is 0, 0.1, 0.3, 0.5, and 1.0 wt % Ni deposited.

before and after photocatalysis indicate an obvious spectral change, which is the CdS absorption edge shifted to a longer wavelength range for the recovery catalyst. It is most likely due to the aggregated CdS particles to stabilize the surface tension to avoid decomposition (Figure S3a,b). Alternatively, it might be due to the oxidized CdS during the recovery process as exposed to air.[30] The photocatalytic H₂ production carried out with the recovery CdS/Ni/KNbO₃ dropped down to 60% of the initial activity (Figure S3c). The XPS spectra in Figure S3d evidently exhibit the electronic status of Cd, S, and Nb comparing before and after photocatalysis. The binding energy of the S 2p and Nb 3p electrons slightly increased for the recovery catalyst, indicating an oxidized status, while the electrons of Cd 3d indicate a reduced electronic status as obtained by the decreased binding energy.

We carried out the measurement of quantum yields, Φ, for the photocatalytic H₂ production of CdS/Ni/KNbO₃ composites. The apparent quantum yield, Φ, for H₂ production is defined as follows:

$$\Phi_{H_2} = d[H_2]/dt/I_a \tag{2}$$

where $d[H_2]/dt$ is the H₂ production rate (mol s^{-1}), and I_a is the number of absorbed photons in units of Einstein s^{-1} from the incident photons flux (I_0) to the system.

The incident photons flux (I_0) is obtained by using the potassium ferrioxalate $[K_2F_2(C_2O_4)_3]$ actinometer with the experimental setup for the photocatalytic hydrogen production reaction.[31,32] The potassium ferrioxalate $[K_2F_2(C_2O_4)_3]$ is transformed to 1−10 phenanthroline $[Fe(phenan)_3]^{2+}$ during photoirradiation, as shown by the optical properties of an actinometer in Figure 8(a). The molar attenuation coefficient of 1−10 phenanthroline $[Fe(phenan)_3]^{2+}$ is determined at 410,
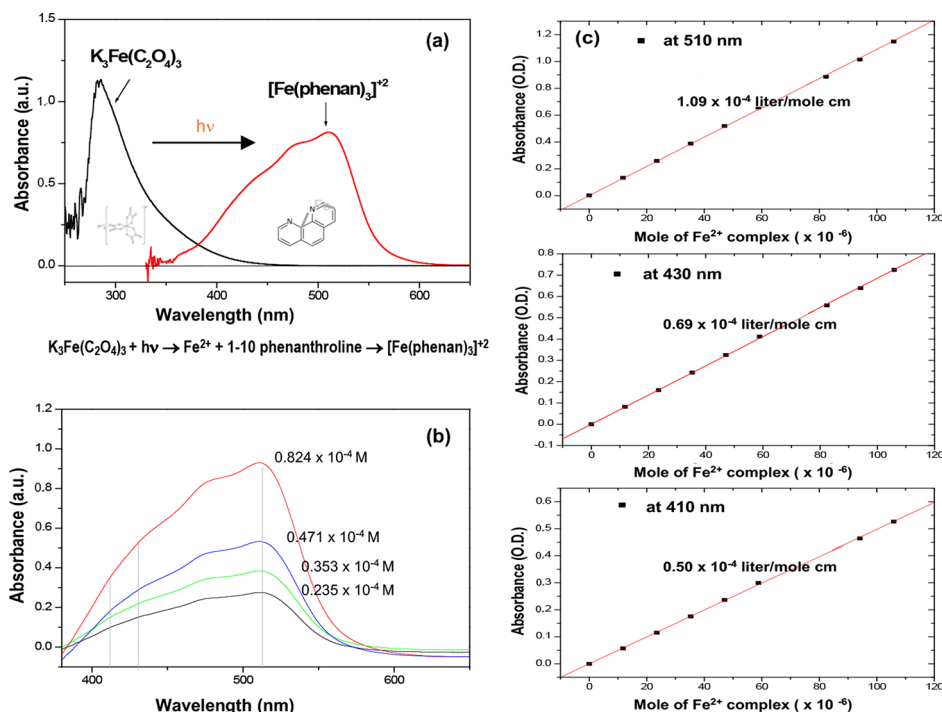
Figure 8. Optical properties of the potassium ferrioxalate actinometer: the potassium ferrioxalate, $[K_2F_2(C_2O_4)_3]$, is transformed to 1−10 phenanthroline, $[Fe(phenan)_3]^{2+}$, by photoirradiation. (a) Absorption spectra of the potassium ferrioxalate and 1−10 phenanthroline that are transformed by photoirradiation. (b) Absorbance of 1−10 phenanthroline, $[Fe(phenan)_3]^{2+}$, that is measured in various concentrations. (c) Molar attenuation coefficient (ε) of $[Fe(phenan)_3]^{2+}$ at the wavelength (λ) of 410, 430, and 510 nm, respectively.

Table 1. Comparison of the Molar Attenuation Coefficient (ε) of CdS Colloid, $K_3Fe(C_2O_4)_3$, and 1−10 Phenanthroline, $[Fe(Phenan)_3]^{2+}$, that Is Obtained at the Common Wavelengths (λ)

λ (nm)	CdS colloid (ε = A l/mol cm)	$K_3Fe(C_2O_4)_3$ (ε = A l/mol cm)	$[Fe(phenan)_3]^{2+}$ (ε = A l/mol cm)
405	7.56×10^{-2}	2.06×10^{-2}	
410	7.06×10^{-2}	1.67×10^{-2}	0.5×10^{-4} $(0.51)^{a}$
430	5.04×10^{-2}	6.6×10^{-3}	0.686×10^{-4} $(0.696)^{a}$
510	8.13×10^{-3}		1.09×10^{-4} $(1.11)^{a}$

^{a}The reference for the (ε) value of $[Fe(phenan)_3]^{2+}$.
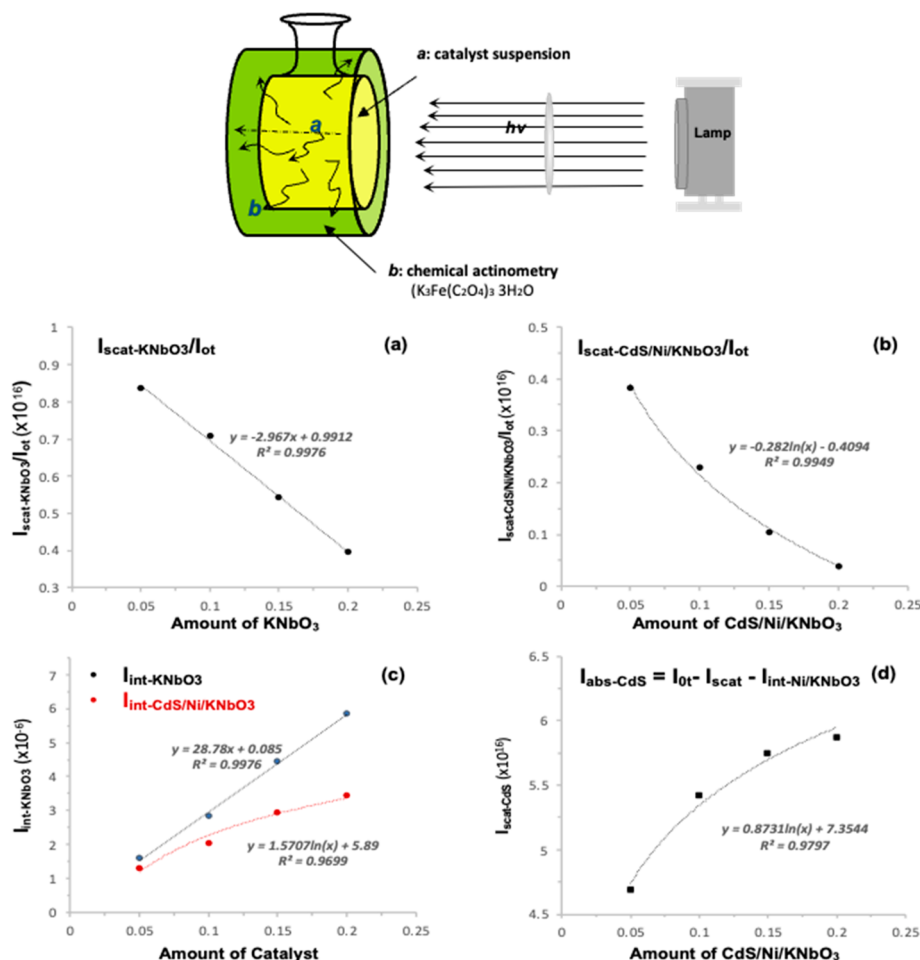
Figure 9. Scheme of the apparatus for a measurement of the scattered light flux from the catalyst (top). The bottom is the plots of the scattered light flux by $KNbO_3$ (a) and $CdS/Ni/KNbO_3$ (b) to the incident light flux (I_{ot}); (c) plot of the internal energy of $KNbO_3$ and $CdS/Ni/KNbO_3$; (d) plot of the absorbed photon flux by CdS with $CdS/Ni/KNbO_3$ corresponding to the catalyst amount of 0.05, 0.1, 0.15, and 0.2 g, respectively.

430, and 510 nm, respectively, with the absorption spectra obtained in the various concentrations, as shown in Figure 8b,c. The comparable molar attenuation coefficients of CdS colloid, $K_3Fe(C_2O_4)_3$, and 1−10 phenanthroline [Fe-(phenan)$_3$]$^{2+}$ are obtained in the common wavelengths as listed in Table 1. As a result, the incident light flux to the photoreactor is defined as $I_0 = 1.27 \times 10^{17}$ quanta/s for visible light ($\lambda \geq 400$ nm) as it is obtained in the absence of photocatalysts.

The $CdS/Ni/KNbO_3$ composites have the particle size around 1 μm. The scattered photon flux (I_{scat}) is calculated by a ferrioxalate $[K_3Fe(C_2O_4)_3]$ actinometry with the specially designed photoreactor, which enables to detect a back- and side-scattered light flux that passed through the photolysis reactor (refer to the apparatus in Figure 9).

The scattered light flux from $KNbO_3$ and $CdS/Ni/KNbO_3$ is obtained with visible light irradiation ($\lambda \geq 400$ nm) corresponding to the catalyst amount of 0.05, 0.10, 0.15, and 0.20 g, respectively, and presented as the plots of I_{scat}/I_{ot} in Figure 9a,b.

Since there is no light absorbance by $KNbO_3$ in the visible light, the difference between the incident (I_{ot}) and the scattered light flux (I_{scat}) is considered as the internal energy of $KNbO_3$ that is consumed as molecular vibrational and rotational modes while showing multiple light scattering among the particles as shown in the equation below.

$$I_{0t} - I_{scat-KNbO_3} = I_{int-KNbO_3} \tag{3}$$

On the other hand, the scattered light flux (I_{scat}) by $CdS/Ni/KNbO_3$ might be a subtraction of the absorbed light flux by CdS nanoparticles ($I_{abs-CdS}$) and the internal energy of Ni/

$KNbO_3$ ($I_{int-Ni/KNbO_3}$) from the incident light flux (I_{ot}). The consumed photons as an internal energy of Ni/$KNbO_3$ ($I_{int-Ni/KNbO_3}$) must be less than that by itself of $KNbO_3$ because a limited surface area of Ni/$KNbO_3$ is exposed to the incident light flux (I_{ot}) due to the CdS nanoparticles deposited on the surface. The impact may increase according to the increased catalyst amount of CdS/Ni/$KNbO_3$. The internal energy of Ni/$KNbO_3$ is estimated to be a logarithmic function corresponding to the increased catalyst amount while the $KNbO_3$ indicates to be a linear function, as shown in Figure 9(c). The absorbed photons by CdS nanoparticles ($I_{abs-CdS}$), which are evaluated as effective and utilizable photons to the photocatalytic H_2 production, are calculated corresponding to the catalyst amount with the equation below and presented the plot in Figure 9(d).

$$I_{abs-CdS} = I_{0t} - (I_{scat} + I_{int-Ni/KNbO_3}) \qquad (4)$$

Since the scattered light flux I_{scat} is dependent on the catalyst amounts corresponding to the incident light flux (I_0), we defined the index for $I_{abs-CdS}$ of CdS/Ni/$KNbO_3$ as the portion of $I_{abs-CdS}$ to I_{0t}. The index is applicable to the designated amounts of CdS/Ni/$KNbO_3$ as listed in Table 2. For example, the index with 0.2 g catalyst amount is defined as 0.605, which means that 0.2 g of CdS/Ni/$KNbO_3$ estimates to absorb and utilize approximately 60.5% of the incident photon flux (I_0) for the photocatalytic molecular hydrogen production. As a result, the absorbed light flux (I_a) by 0.2 g of CdS/Ni/$KNbO_3$ including 2.9 wt % CdS and 0.1 wt % Ni indicates approximately $7.68 × 10^{16}$ quanta/s after applying the index of 0.605 to the incident light flux (I_0) of $1.27 × 10^{17}$ ($λ ≥ 400$ nm) to the photoreactor. The corresponding quantum yield for the photocatalytic hydrogen generation of ~40 $μ$mol/h under visible light ($λ ≥ 400$ nm) is determined as 8.8% in 30% IPA aqueous solution from the equation, $\Phi_{H_2} = d[H_2]/dt × (6.023 × 10^{23})/I_a$.

4. CONCLUSIONS

In this study, we investigate the structural properties of $KNbO_3$ comparing the stoichiometric and nonstoichiometric $KNbO_3$ structure corresponding to Ni deposit, and the photophysical properties and photocatalytic activity of CdS/Ni/$KNbO_3$ composites as well.

The FTIR spectral analysis comparing the stoichiometric (1:1) and nonstoichiometric (1:1.1) $KNbO_3$ structure reveals the different aspects of the deposited Ni effects corresponding to the structure. The nonstoichiometric structure of $KNbO_3$(1:1.1) generates the defects at the K^+ site, which is Ni-occupied during its deposit process. It exhibits a tendency like a doped Ni into $KNbO_3$ up to 0.1 wt % of Ni and then forms a Ni cluster in case the amount exceeds 0.1 wt %. The photophysical properties of CdS/Ni/$KNbO_3$ examined with UV−vis absorption and luminescence spectral analysis demonstrates the CdS/Ni/$KNbO_3$ composites to be efficient light conversion caused by efficient charge/electron transfer between $KNbO_3$ and CdS via doped Ni.

The photocatalytic activity of CdS/Ni/$KNbO_3$ exhibits a CdS and Ni amount dependency. The best photocatalytic activity for H_2 generation is obtained with 0.1 wt % Ni and 2.9 wt % CdS composite as it gradually declines with the excess Ni amounts than 0.1 wt % caused by a formed Ni cluster.

Table 2. Scattered (I_{scat}) and the Absorbed Photon Flux (I_a) Corresponding to $KNbO_3$ and CdS/Ni/$KNbO_3$ Amount with the Portion to the Incident Light Flux as I_{scat}/I_{ot} (%) and I_a/I_{ot}[a,b]

catalyst (amount)		I_{scat} 0.05 g	0.10 g	0.15 g	0.20 g	I_{scat}/I_{0t} (%) 0.05 g	0.10 g	0.15 g	0.20 g	I_a/I_{0t} 0.05 g	0.10 g	0.15 g	0.20 g
$KNbO_3$	I_{scat}	$8.1 × 10^{16}$	$6.87 × 10^{16}$	$5.26 × 10^{16}$	$3.84 × 10^{16}$	83.5	70.8	54.2	39.6	$1.6 × 10^{16}$ (16.5%)	$2.83 × 10^{16}$ (29.2%)	$4.44 × 10^{16}$ (45.8%)	$5.86 × 10^{16}$ (60.4%)
	$I_{int-KNbO_3}$												
CdS/Ni/$KNbO_3$	I_{scat}	$3.71 × 10^{16}$	$2.22 × 10^{16}$	$1.01 × 10^{16}$	$3.70 × 10^{15}$	38.2	22.9	10.4	3.8				
	$I_{int-Ni/KNbO_3}$									$1.3 × 10^{16}$	$2.03 × 10^{16}$	$2.94 × 10^{16}$	$3.46 × 10^{16}$
	$I_{abs-CdS}$									$4.69 × 10^{16}$ (48.4%)	$5.45 × 10^{16}$ (56.2%)	$5.75 × 10^{16}$ (59.3%)	$5.87 × 10^{16}$ (60.5%)
index (I_a)[c] of CdS/Ni/$KNbO_3$										0.484	0.562	0.593	0.605

[a]The portion of the CdS absorbed photons to the incident light flux ($I_{abs-CdS}/I_{0t}$) is determined as the index (I_a)[c], which is applicable to the designated CdS/Ni/$KNbO_3$ catalyst amount for a quantum yield measurement. $I_{0t} = 9.7 × 10^{17}$ quanta/s, when $(1 − 10^{−ε[A]l}) = 1$. [b]I_{scat} by $KNbO_3$ = $I_{scat-KNbO_3} = I_{0t} − I_{scat-KNbO_3}$; $I_{abs-KNbO_3(λ > 400nm)} = I_{int-KNbO_3}$; I_{scat} by CdS/Ni/$KNbO_3$ = $I_{scat-CdS/Ni/KNbO_3} = I_{0t} − (I_{int-Ni/KNbO_3} − I_{abs-CdS})$; $I_{0t} − (I_{int-Ni/KNbO_3} + I_{abs-CdS})$; $I_{abs-CdS/Ni/KNbO_3(λ > 400nm)} = I_{int-Ni/KNbO_3} − I_{int-Ni/KNbO_3}$; $I_{scat-CdS/Ni/KNbO_3} = I_{0t} − (I_{int-Ni/KNbO_3} − I_{abs-CdS})$. [c]Index I_a of CdS/Ni/$KNbO_3$ is the portion of $I_{abs-CdS}$ to I_{0t} corresponding to the catalyst amount.

■ ASSOCIATED CONTENT

ⓢ Supporting Information

The Supporting Information is available free of charge at https://pubs.acs.org/doi/10.1021/acsomega.3c04829.

Comparative XRD pattern of the stoichiometric $KNbO_3$ (1:1) and the nonstoichiometric $KNbO_3$ (1:1.1) structure; TEM image of CdS nanoparticles distributed on the surface of $KNbO_3$; comparative UV−vis absorption and XPS spectra of $CdS/Ni/KNbO_3$ composites before and after 24 h photocatalysis with the photocatalytic H_2 production rates (PDF)

■ AUTHOR INFORMATION

Corresponding Authors

Su Young Ryu − *Environmental Science & Engineering, Linde Laboratory, California Institute of Technology, Pasadena, California 91125, United States;* ⓞ orcid.org/0000-0002-3246-6126; Phone: 1-626-395-4391; Email: syryu7@gmail.com; Fax: 1-626-395-2940

Michael R. Hoffmann − *Environmental Science & Engineering, Linde Laboratory, California Institute of Technology, Pasadena, California 91125, United States;* ⓞ orcid.org/0000-0001-6495-1946; Phone: 1-626-395-4391; Email: mrh@caltech.edu; Fax: 1-626-395-2940

Author

Tai Kyu Lee − *Nanopac Co., Ltd., Yongin-si, Gyeonggi-do 17015, Republic of Korea*

Complete contact information is available at:
https://pubs.acs.org/10.1021/acsomega.3c04829

Author Contributions

S.Y.R. performed the research, data analysis, and wrote the manuscript. M.R.H., the lab director and supervising professor, reviewed the manuscript.

Notes

The authors declare no competing financial interest.

■ ACKNOWLEDGMENTS

■ REFERENCES

(1) Fujishima, A.; Honda, K. Electrochemical Photolysis Water at a Semiconductor Electrode. *Nature* **1972**, *238*, 37−38.

(2) Kudo, A.; Sayama, K.; Tanaka, A.; Asakura, K.; Domen, K.; Maruya, K.; Onishi, T. Nickel-loaded $K_4Nb_6O_{17}$ Photocatalyst in the Decomposition of H_2O into H_2 and O_2: Structure and Reaction Mechanism. *J. Catal.* **1989**, *120*, 337−352.

(3) Sayama, K.; Tanaka, A.; Domen, K.; Maruya, K.; Onishi, T. Photocatalytic Decomposition of Water over Platinum-Intercalated $K_4Nb_6O_{17}$. *J. Phys. Chem.* **1991**, *95*, 1345−1348.

(4) Sayama, K.; Yase, K.; Arakawa, H.; Asakura, K.; Tanaka, A.; Domen, K.; Onishi, T. Photocatalytic Activity and Reaction Mechanism of Pt-intercalated $K_4Nb_6O_{17}$ Catalyst on the Water Splitting in Carbonate Salt Aqueous Solution. *J. Photochem. Photobiol. A Chem.* **1998**, *114*, 125−135.

(5) Kudo, A.; Tanaka, A.; Domen, K.; Maruya, K.-I.; Aika, K.-I.; Onishi, T. Photocatalytic Decomposition of Water over NiO-$K_4Nb_6O_{17}$ Catalyst. *J. Catal.* **1988**, *111*, 67−76.

(6) Kato, H.; Kobayashi, H.; Kudo, A. Role of Ag^+ in the Band Structures and Photocatalytic Properties of $AgMO_3$ (M: Ta and Nb) with the Perovskite Structure. *J. Phys. Chem. B* **2002**, *106*, 12441−12447.

(7) Shangguan, W. F.; Yosida, A. Photocatalytic Hydrogen Evolution from Water on Nanocomposites Incorporating Cadmium Sulfide into the Interlayer. *J. Phys. Chem. B* **2002**, *106*, 12227−12230.

(8) Li, Q.; Li, X.; Yu, J. Surface and Interface Modification Strategies of CdS-based Photocatalysts. *Interface Sci. Technol.* **2020**, *31*, 313−348.

(9) Meng, A.; Zhu, B.; Zhong, B.; Zhang, L.; Cheng, B. Direct Z-scheme TiO_2/CdS Hierarchical Photocatalyst for Enhanced Photocatalytic H_2-Production Activity. *Appl. Surf. Sci.* **2017**, *422*, 518−527.

(10) Innocenti, M.; Cattalin, S.; Loglio, F.; Cecconi, T.; Seravalli, G.; Foresti, M. L. Ternary Cadmium and Zinc Sulfides: Composition, Morphology and Photoelectrochemistry. *Electrochim. Acta* **2004**, *49*, 1327−1337.

(11) Zhang, J. L.; Xiao, M.; Liu, Z. M.; Han, B. X.; Jiang, T.; He, J.; Yang, G. Y. Preparation of ZnS/CdS Composite Nanoparticles by Coprecipitation from Reverse Micelles using CO_2 as Antisolvent. *J. Colloid Interface Sci.* **2004**, *273*, 160−164.

(12) Shangguan, W. F.; Yosida, A. Synthesis and Photocatalytic Properties of CdS-intercalated Metal Oxides. *Sol. Energy Mater. Sol. Cells* **2001**, *69*, 189−194.

(13) Yoshimura, J.; Tanaka, A.; Kondo, J. N.; Domen, K. Visible Light Induced Hydrogen Evolution on $CdS/K_4Nb_6O_{17}$ Photocatalyst. *Bull. Chem. Soc. Jpn.* **1995**, *68*, 2439−2445.

(14) Wu, X.; Zhao, J.; Wang, L.; Han, M.; Zhang, M.; Wang, H.; Huang, H.; Liu, Y.; Kang, Z. Carbon Dots as Solid-State Electron Mediator for $BiVO_4$/CDs/CdS Z-scheme Photocatalyst Working under Visible Light. *Appl. Catal. B: Environ.* **2017**, *206*, 501−509.

(15) Ng, B.-J.; Putri, L. K.; Kong, X. R.; Teh, Y. W.; Pasbakhsh, P.; Chai, S.-P. Z-Scheme Photocatalytic Systems for Solar Water Splitting. *Adv. Sci.* **2020**, *7*, No. 1903171.

(16) Duan, C.-G.; Mei, W. N.; Liu, J.; Hardy, J. R. First-principles Study on the Optical Properties of $KNbO_3$. *J. Phys.: Condens. Matter* **2001**, *13*, 8189−8195.

(17) Neumann, T.; Borstel, G.; Scharfschwerdt, C.; Neumann, M. Electronic Structure of $KNbO_3$ and $KTaO_3$. *Phys. Rev. B* **1992**, *46*, 10623−10628.

(18) Bussière, G.; Reber, C. Coupled Excited States in Nickel (II) Complexes Probed by Polarized Absorption Spectroscopy. *J. Am. Chem. Soc.* **1998**, *120*, 6306−6315.

(19) Bunker, P. R.; Jensen, P. *Molecular Symmetry and Spectroscopy*; NRC Research Press: NRC, Canada, 2006, 414. ISBN 978-0660196282.

(20) Low, W. Paramagnetic and Optical Spectra of Divalent Nickel in Cubic Crystalline Fields. *Phys. Rev.* **1958**, *109*, 247−255.

(21) Domingo, A.; Rodríguez-Fortea, A.; Swart, M.; de Graaf, C.; Broer, R. Ab initio Absorption Spectrum of NiO Combining Molecular Dynamics with the Embedded Cluster Approach in a Discrete Reaction Field. *Phys. Rev. B* **2012**, *85*, No. 155143.

(22) Papavassiliou, G. C. Surface Plasmons in Small Au-Ag Alloy Particles. *J. Phys. F: Met. Phys.* **1976**, *6*, L103.

(23) Schmidt, F.; Landmann, M.; Rauls, E.; Argiolas, N.; Sanna, S.; Shmidt, W. G.; Schindlmayr, A. Consistent Atomic Geometries and Electronic Structure of Five Phases of Potassium Niobate from Density-Functional Theory. *Adv. Mater. Sci. Eng.* **2017**, *2017*, No. 3981317.

(24) Ryu, S. Y.; Choi, J.; Balcerski, W.; Lee, T.-K.; Hoffmann, M. R. Photocatalytic Production of H_2 on Nanocomposite Catalysts. *Ind. Eng. Chem. Res.* **2007**, *46*, 7476−7488.

(25) Wu, Y.; Chan, M. K. Y.; Ceder, G. Prediction of Semiconductor Band Edge Positions in Aqueous Environments from First Principles. *Phys. Rev. B* **2011**, *83*, No. 235301.

(26) Grigorjeva, L.; Millers, D.; Popov, A. I.; Kotomin, E. A.; Polzik, E. S. Luminescence Properties of $KNbO_3$ Crystals. *J. Lumin.* **1997**, *72-74*, 672−674.

(27) Kamalov, V. F.; Little, R.; Logunov, S. L.; El-Sayed, M. A. Picosecond Electronic Relaxation in CdS/HgS/CdS Quantum Dot Quantum Well Semiconductor Nanoparticles. *J. Phys. Chem.* **1996**, *100*, 6381−6384.

(28) Veamatahau, A.; Jiang, B.; Seifert, T.; Makuta, S.; Latham, K.; Kanehara, M.; Teranishi, T.; Tachibana, Y. Origin of Surface Trap States in CdS quantum Dots: Relationship Between Size Dependent Photoluminescence and Sulfur Vacancy Trap States. *Phys. Chem. Chem. Phys.* **2015**, *17*, 2850−2858.

(29) Kamat, P. V.; Shanghavi, B. Interparticle Electron Transfer in Metal/Semiconductor Composites. Picosecond Dynamics of CdS-Capped Gold Nanoclusters. *J. Phys. Chem. B* **1997**, *101*, 7675−7679.

(30) Ryu, S. Y.; Balcerski, W.; Lee, T. K.; Hoffmann, M. R. Photocatalytic Production of Hydrogen from Water with Visible Light Using Hybrid Catalysts of CdS Attached to Microporous and Mesoporous Silicas. *J. Phys. Chem. C* **2007**, *111*, 18195−18203.

(31) Hatchard, C. G.; Parker, C. A. A New Sensitive Chemical Actinometer. II. Potassium Ferrioxalate as a Standard Chemical Actinometer. *Proc. R Soc. Lond. A Math. Phys. Sci.* **1956**, *A235*, 518−536.

(32) Cornu, C. J. G.; Colussi, A. J.; Hoffmann, M. R. Quantum Yields of the Photocatalytic Oxidation of Formate in Aqueous TiO_2 Suspensions under Continuous and Periodic Illumination. *J. Phys. Chem. B* **2001**, *105*, 1351−1354.